Theoretical and Applied Climatology (2019) 136:119–134
https://doi.org/10.1007/s00704-018-2471-z

ORIGINAL PAPER

A possible recovery of the near-surface wind speed in Eastern China during winter after 2000 and the potential causes

Jinlin Zha[1] · Jian Wu[1] · Deming Zhao[2] · Jianping Tang[3]

Received: 11 August 2017 / Accepted: 28 March 2018 / Published online: 14 April 2018

Abstract

A lasting decrease in the near-surface wind speed (SWS) in China has been revealed, but a following short-term strengthening in the SWS was rarely noted. In this paper, the daily mean SWS observed datasets from 328 measurement stations in Eastern China during the period 1981–2011 were used to investigate the facts and causes of the observed short-term strengthening in winter SWS in recent decades. The major results are summarized as follows: the SWS showed a significant decrease in the last 30 years, but a short-term strengthening in SWS was observed during the winter since 2000 in Eastern China. The SWS in Eastern China showed a significant decrease of − 0.11 m s^{-1} $decade^{-1}$ from 1981 to 1999, followed by a weak increase of 0.0008 m s^{-1} $decade^{-1}$ from 2000 to 2011. The short-term strengthening in the SWS since 2000 was mainly induced by the changes of the pressure-gradient force (PGF), which could be attributed to the changes of the sea-level pressure (SLP) in the region (51°–69.75° N, 51.75°–111.75° E). Furthermore, the changes of the PGF during the two periods of 1981–1999 and 2000–2011 were consistent with those of the SLP in the region (51°–69.75° N, 51.75°–111.75° E). The correlation coefficient between PGF and SLP was 0.32 and 0.66 during the period 1981–1999 and 2000–2011, respectively. Therefore, the effects of the changes in SLP over the region (51°–69.75° N, 51.75°–111.75° E) on changes of SWS in the Eastern China should be significant.

1 Introduction

The Earth's atmosphere redistributes heat fluxes originated from incoming solar radiation through global and regional circulations. Atmospheric circulations involve movement of air mass, namely wind, which helps prevent dramatic changes in air and surface temperature across latitudes (Kim and Paik 2015). As we know, long-term changes in near-surface wind speed (SWS) could affect water vapor evaporation and hydrological cycles (Liu et al. 2010; McMahon et al. 2013; Liu and McVicar 2012; McVicar et al. 2012), visibility, aerosol distribution, and air quality (Lin et al. 2015) as well as distribution of wind energy (Karnauskas et al. 2017). Furthermore, SWS changes can also influence crop water requirement, and changes of this parameter can in turn affect the potential reference crop evapotranspiration. Therefore, SWS change is a crucial factor in water resource management (Dinpashoh 2006; Dinpashoh et al. 2011). In a word, it is very important to study the changes of SWS and discuss the potential causes of changes in SWS.

A significant decreasing trend has been discovered in many regions, in which 5–15% reduction in SWS was reported over almost all continental regions in the northern mid-latitudes over the past 30 years, with linearly decreasing trends in Europe, Middle Asia, East Asia, South Asia, and North America of − 0.09, − 0.16, − 0.12, − 0.08, and − 0.07 m s^{-1} $decade^{-1}$, respectively (Vautard et al. 2010). The slowdown in land surface wind speed across the globe was also revealed in other studies (Vautard et al. 2012; Tobin et al. 2014; Berrisford et al. 2015; Dunn et al. 2016). In Europe, the slowdown in SWS was mainly observed in the Iberian Peninsula from 1992 to 2006 (Garcia-Bustamante et al. 2012), in Switzerland from 1983 to 2006, in the Netherlands during the period 1970–2010 (Cusack 2013), and in Portugal and Spain during the period 1979–2008

✉ Jian Wu
wujian@ynu.edu.cn

[1] Key Laboratory of Atmospheric Environment and Processes in the Boundary Layer over the Low-Latitude Plateau Region, Department of Atmospheric Science, Yunnan University, Kunming 650091, China

[2] CAS Key Laboratory of Regional Climate-Environment for Temperate East Asia, Institute of Atmospheric Physics, Chinese Academy of Sciences, Beijing 100029, China

[3] School of Atmospheric Science, Nanjing University, Nanjing 210000, China

(Azorin-Molina et al. 2014). In North America, a reduction in SWS was mainly reported in Canada and America (Wan et al. 2010; Pryor et al. 2009; Pryor and Ledolter 2010; Greene et al. 2012). In Asia, a decrease in SWS was mainly found in India (Bandyopadhyay et al. 2009), Japan (Fujibe 2009), and South Korea (Kim and Paik 2015). A distinct decrease in the SWS was also found in China (Xu et al. 2006; Jiang et al. 2010; You et al. 2010; Fu et al. 2011; Guo et al. 2011; Lin et al. 2013; Zha et al. 2017a, b).

The long-term decrease of SWS has been widely reported in the former studies, but the causes of the slowdown in SWS were not clear. Due to the correlation between increasing temperature and decreasing SWS, some studies tended to explain the decrease of SWS as a result of temperature increase (Fujibe 2009; Dadaser-Celik and Cengiz 2014). The decrease of SWS was also linked to changes of circulation patterns in different areas, for example, the Arctic oscillation (AO) and North Atlantic oscillation (NAO) (Clifton and Lundquist 2012; Jerez et al. 2013; Azorin-Molina et al. 2014, 2016), East Asian monsoon (Xu et al. 2006), and Pacific decadal oscillation (PDO) (Fu et al. 2011). Nevertheless, some studies also revealed that the slowdown in SWS was induced by the increase in surface roughness attributed to land use and cover change (LUCC) (Vautard et al. 2010; Bichet et al. 2012; Wu et al. 2016, 2017a, b, c; Zha et al. 2016, 2017a, b).

Relative to the well-documented decrease in SWS, the observed short-term recovery of SWS and potential causes were rarely involved in previous studies. Kim and Paik (2015) reported a slowdown during the decreasing trend in the SWS in South Korea during the period 1990–2002 and a rise in the seasonal mean SWS after 2003 in summer. Guo et al. (2011) noted a slowdown during the decreasing process of annual and seasonal mean SWS in China after 1991. Yang et al. (2012) found a pronounced increase in the annual and seasonal mean SWSs in southwestern China after 2000. Lin et al. (2013) reported a recovery of wind speed over the Tibetan Plateau (TP) since the beginning of the 2000s and proposed that the recovery might be a precursor of a trend reversal of wind speed over China.

The reasons of the decrease in SWS have been discussed from different viewpoints in the previous studies; otherwise, the causes of the recovery in SWS observed at some regional scales were rarely explored. Therefore, the primary aims of this study include the following: (1) to reveal the phenomenon of the short-term recovery of SWS and discuss the potential causes of the recovery in SWS during winter over Eastern China after 2000; (2) to investigate the potential causes of the changes in pressure-gradient force (PGF) over the study region; and (3) to detect the spatio-temporal characteristics of monthly changes of sea-level pressure (SLP). The data and methods used in this study are presented in Section 2, followed by the characteristics of the possible recovery after a significant decrease in the SWS in Section 3. Further in-depth discussion is given in Section 4, and a summary of the findings is given in Section 5.

2 Data and methods

2.1 Data

The study region is Eastern China (15°–55° N, 108°–135° E) due to its high density of meteorological stations and mostly flat topography, and daily mean SWS data of 328 stations in Eastern China during the period 1980–2011 is analyzed in this study, which were selected according to the following two criteria: (1) It is a standard national meteorological station, and the station did not relocate in the study period; (2) the observation of SWS began since 1980, and the total days of missing data should be less than 1% of the length of total data series at each station. The spatial pattern of the total 328 stations and terrain height in the Eastern China are shown in Fig. 1. The wind speed was measured with anemometer 10 m above the ground, and at the same time, the siting, installation, and observation of the anemometer conformed the standard of the World Meteorological Organization's Guide to Global Observation System and China Meteorological Administration's Technical Regulations on Weather Observation (CMA 2003; Fu et al. 2011; Guo et al. 2011). In addition, Liu (2000) examined the credibility of annual mean SWS in China in the last 40 years using the standard normal homogeneity (SNHT) method and indicated that this SWS dataset was credible. Furthermore, the wind speed dataset has been used many times in our previous studies (Zha et al. 2017a, b). To calculate the PGF, the daily mean air temperature, water vapor pressures, and air pressures in winter are also used in this study. The continuity of these dataset is good, with only a few stations having non-continuous records. These datasets were operated, provided, and quality tested by the National Meteorological Information Center (NMIC) of the China Meteorological Administration (CMA 2003). Therefore, they are considered to be credible dataset.

The SLP located in the region, 0°–75° N, 49.5°–180° E, was also used to investigate the cause of the changes in PGF over Eastern China. The SLP measured four times per day (at UTC 00, 06, 12, and 18) from the European Centre for Medium-Range Weather Forecasts (ECMWF) reanalysis from January 1989 onward (to be extended back to January 1979) (ERA-Interim) dataset at a 0.75° × 0.75° resolution. The ERA-Interim dataset was produced with a sequential four-dimensional variational assimilation scheme (Dee et al. 2011). A comparison with the ERA-40 dataset, the representation of the hydrological cycle, the quality of the stratospheric circulation data, and the consistency in time of the reanalysis fields was improved in the ERA-Interim dataset (Dee et al.

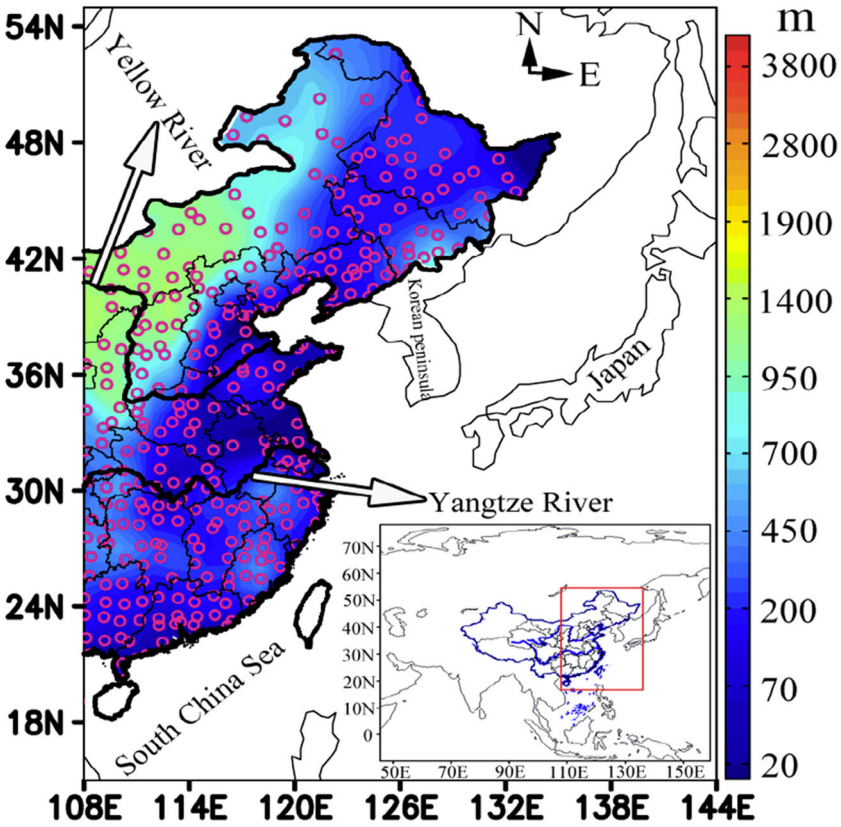

Fig. 1 Terrain height and stations location in Eastern China. Red circles denote the 328 surface weather stations, and the bar denotes the terrain altitude

2011). Details about the ERA-Interim reanalysis dataset can be found in Simmons et al. (2007, 2010, 2014).

2.2 Methods

The calculation method of PGF has been expressed in our previous study (Wu et al. 2016), and we just simply present main steps of the method to keep completeness. The PGF, denoted by , can be calculated in a Sigma-spherical coordinate system using air pressure and other meteorological elements observed at each station, which is expressed by Eq. (1):

$$\overrightarrow{G} = -\nabla_\sigma \Phi - \frac{RT}{P_s}\nabla P_s \tag{1}$$

where P_s is the observed surface pressure (unit: Pa), T is the observed air temperature (unit: K), Φ is the gravitational potential (unit: $m^2\ s^{-2}$). R is air constant including the effect of water vapor (unit: J kg^{-1} K^{-1}), which can be denoted by Eq. (2):

$$R = \left(1 + \frac{0.378e}{P_s - 0.378e}\right)\cdot R_d \tag{2}$$

where e is the observed water vapor pressure (unit: Pa), R_d is the gas constant of dry air, and $R_d = 287.05$ J $kg^{-1}K^{-1}$. Equation (1) could be unfolded in the spherical coordinate system, and the vertical components are neglected, defined by Eq. (3):

$$-\nabla_\sigma \Phi - \frac{RT}{P_s}\nabla p_s = -\left(\frac{\partial \Phi}{r\cos\varphi\partial\lambda} + \frac{\partial P_s}{\rho r\cos\varphi\partial\lambda}\right)_\sigma \vec{i} - \left(\frac{\partial \Phi}{r\partial\varphi} + \frac{\partial P_s}{\rho r\partial\varphi}\right)_\sigma \vec{j} \tag{3}$$

where r is the radius of the Earth (unit: m), and φ and λ are the latitude and longitude, respectively. ρ is the air density, $\rho = \frac{P_s}{RT}$. The four-order difference scheme, expressed by Eq. (4), is used to calculate the longitudinal and the latitudinal differences in Eq. (3) (Wu et al. 2016):

$$\begin{aligned}\left(\frac{\partial H}{\partial\lambda}\right) &= \frac{4}{3}\left(\frac{H_{i,j+1} - H_{i,j-1}}{2\Delta\lambda}\right) - \frac{1}{3}\left(\frac{H_{i,j+2} - H_{i,j-2}}{4\Delta\lambda}\right) + O(\Delta^4\lambda)\\ \left(\frac{\partial H}{\partial\varphi}\right) &= \frac{4}{3}\left(\frac{H_{i+1,j} - H_{i-1,j}}{2\Delta\varphi}\right) - \frac{1}{3}\left(\frac{H_{i+2,j} - H_{i-2,j}}{4\Delta\varphi}\right) + O(\Delta^4\varphi)\end{aligned} \tag{4}$$

where $H = \Phi$ or P_s, i and j denote the latitudinal and longitudinal component of Φ and P_s, $O(\Delta^4\lambda)$ and $O(\Delta^4\varphi)$ is the truncation error. The values of P_s, T, e, φ, and λ can be observed in the meteorological station, so the value of PGF can be calculated. The details about the calculation of PGF can also be found in Wu et al. (2016).

The classical Mann-Kendall method was used to examine the long-term changes of SWS. Some previous studies have

revealed that the influence of auto-correlation of time series on the Mann-Kendall test is evident (Yue and Wang 2002; Kumar et al. 2009; Dinpashoh et al. 2014), so the Mann-Kendall method following the removal of the effect of significant lag-one auto-correlation is used to eliminate the influence of serial correlation on the Mann-Kendall test. In order to facilitate describing, the classical Mann-Kendall method is named as MK1, and the Mann-Kendall method following the removal of the effect of significant lag-one auto-correlation is named as MK2. In some recent studies, the MK2 was used to determine trends in climatic dataset (Aziz and Burn 2006; Birsan et al. 2005; Novotny and Stefan 2007). The details about MK2 can be found in Kumar et al. (2009) and Dinpashoh et al. (2014). The linear trend coefficient is calculated using the least-squares method (LSM), and the Student's t test is used to determine the significance of the data. In order to compare with LSM, the non-parametric Theil-Sen approach (TSA) is also used in this study (Thiel 1950; Sen 1968). In addition, the Cressman objective analysis method is used to interpolate the station observational data to grids at a resolution of 0.75° to calculate the PGF (Cressman 1959). This method is widely used in climate analysis, numerical weather predictions, and data assimilation systems (Sinha et al. 2006; Narkhedkar et al. 2008). The bilinear interpolation method is used to interpolate the grid data to the 328 observation stations, and this method has also been judged to be least suitable for the transfer of a grid forecast field to another or discrete observation field (Mastylo 2013; Wu et al. 2016). A Gaussian low-pass filter is used to determine the inter-decadal changes in the data (Li et al. 2010, 2011; Zhu et al. 2012).

3 Results and analysis

3.1 Temporal changes of seasonal mean wind speeds

An observed significant decrease in the annual mean SWS over Eastern China has been well documented (Guo et al. 2011; Zha et al. 2017a, b), and a similar fact was observed in the seasonal mean SWS over Eastern China (Fig. 2). The seasonal SWS in Eastern China presented a significant annual fluctuation from 1981 to 2011, associating a long-term fluctuant decrease indicated by the 9-year low-pass-filtered time series by a Gaussian-type filter. In addition, the averaged wind speed was 1.82, 2.70, 2.21, and 2.23 m s^{-1} during winter, spring, summer, and autumn, respectively. At the same time, the SWS showed downward trends in the four seasons in the last 30 years, and the weakest decreasing trend was observed during winter and summer (− 0.09 m s^{-1} $decade^{-1}$; $p < 0.01$ level) (Fig. 2a, c) and the strongest decreasing trend was observed during spring (− 0.14 m s^{-1} $decade^{-1}$; $p < 0.01$ level) (Fig. 2b). Furthermore, the average decreasing trend during 1980–1999 was larger than that of the whole study period, and all linear trends passed the significant t test at the 99% confidence level. After 1999, the SWS showed a downward trend during spring, summer, and autumn, with a rate of − 0.17, − 0.14, and − 0.16 m s^{-1} $decade^{-1}$, respectively, and these decreasing trends passed the significant t test at the 95% confidence level (Fig. 2b–d). A weak increasing rate of 0.0008 m s^{-1} $decade^{-1}$ in SWS was found from 2000 to 2011, and although this linear trend rate failed to pass the significant t test at 99% significance level, this stage of rise still formed a distinct contrast to the previous long-term decrease in SWS. In order to compare with the LSM, the non-parametric TSA is used to calculate the slope of SWS (Thiel 1950; Sen 1968), and the results are shown in Table 1. The results indicated that the trends computed using the LSM were similar to that computed using the TSA during the three time periods (Table 1). The maximum difference of slope was only 0.0018 m s^{-1} a^{-1}. Furthermore, during the two periods 1981–1999 and 1981–2011, all slopes were negative in the all four seasons. During the period 2000–2011, the negative slopes could be found both in LSM and TSA in spring, summer, and autumn, except for in winter. Therefore, from 2000 to 2011, the changes of SWS in winter were not consistent with those in other three seasons, and the increasing trend of SWS could be revealed in both LSM and TSA. These results implied that the changes of SWS during winter were not consistent with those during the other three seasons after 1999, and a short-term strengthening of winter SWS could occur after 1999.

The Mann-Kendall test was used to examine the temporal changes of seasonal SWS. The results showed that a lasting decrease of the SWS during winter was revealed from 1981 to 2000 based on MK1 and MK2, in which a statistically significant decrease was revealed during 1981–1987 and 1992–1995 based on MK1 and during 1981–1992 based on MK2 (Fig. 2e). In addition, an increasing trend in the SWS during winter was discovered after 2000 based on both MK1 and MK2, although this increasing trend failed to pass the significant t test at 95% level. According to the Mann-Kendall test, a turning point in the SWS from a decrease to an increase appeared at 2000. In the other three seasons, the SWS showed a decreasing trend during the study period, and the decreasing trend was significant in spring between 1981–2001 and 1981–1994 based on MK1 and MK2, respectively (Fig. 2f); in summer between 1981–2006 and 1981–1989 based on MK1 and MK2, respectively (Fig. 2g); and in autumn between 1981–2000 and 1981–1991 based on MK1 and MK2, respectively (Fig. 2h), but a possible recovery of SWS could not be observed after 1999 in these three seasons. The

Fig. 2 Temporal changes of seasonal SWS during the period 1981–2011 and the Mann-Kendall test of the seasonal SWS. **a**–**d** Winter, spring, summer, autumn, respectively. The green lines in **a**–**d** denote a 9-year low-pass-filtered time series with a Gaussian-type filter. The black, blue and red lines in **a**–**d** denote the linear fitting curves of SWS during the periods 1981–2011, 1981–1999, and 2000–2011, respectively. R is the correlation coefficient, and R_c is the threshold of significant t test at the 99% confidence level. (The blue lines in **e**–**h** denote the threshold of the significance at the 95% confidence level)

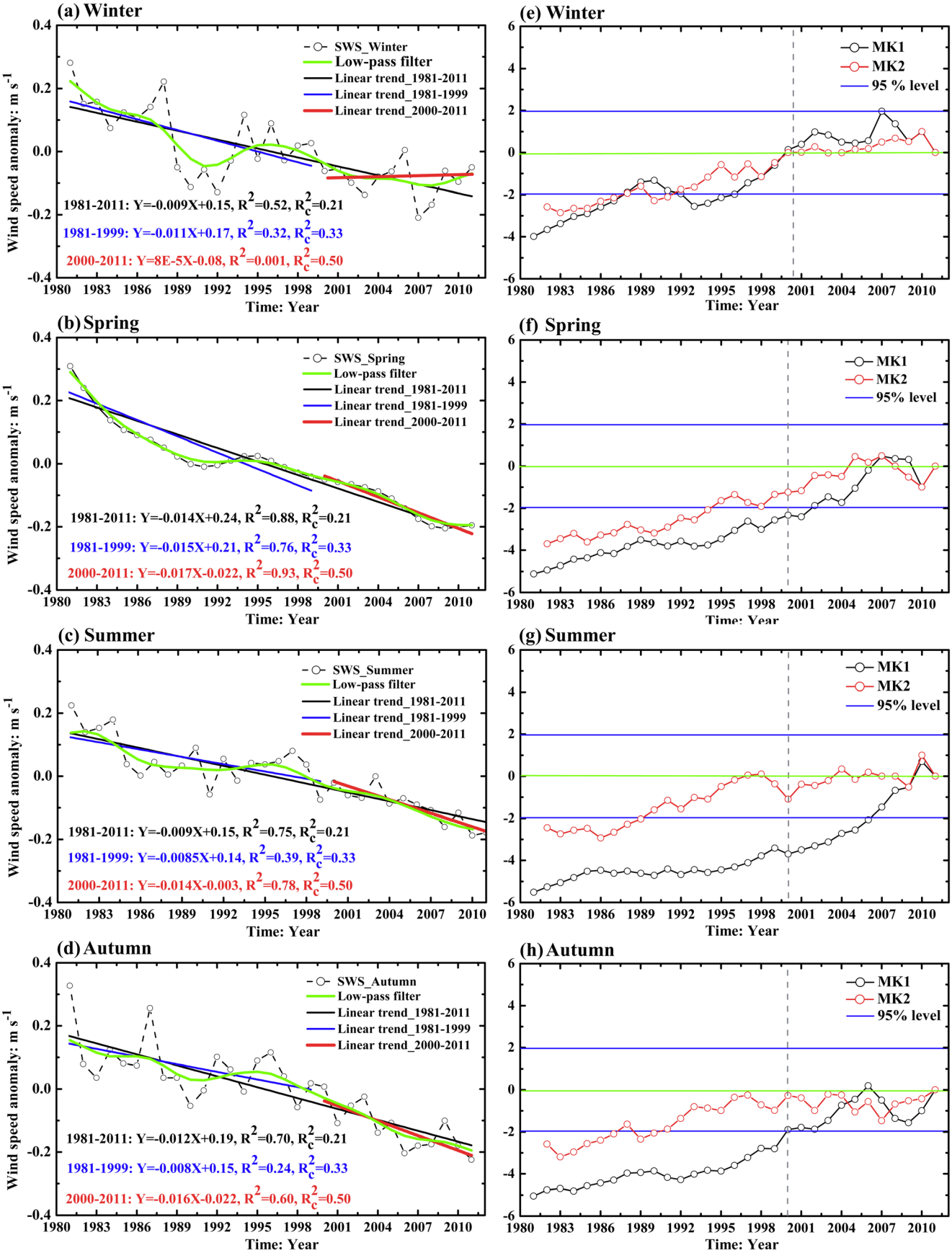
(a) Winter
SWS_Winter
Low-pass filter
Linear trend_1981-2011
Linear trend_1981-1999
Linear trend_2000-2011
1981-2011: Y=-0.009X+0.15, R2=0.52, Rc2=0.21
1981-1999: Y=-0.011X+0.17, R2=0.32, Rc2=0.33
2000-2011: Y=8E-5X-0.08, R2=0.001, Rc2=0.50
Wind speed anomaly: m s-1
Time: Year
(e) Winter
MK1
MK2
95 % level
Time: Year
(b) Spring
SWS_Spring
Low-pass filter
Linear trend_1981-2011
Linear trend_1981-1999
Linear trend_2000-2011
1981-2011: Y=-0.014X+0.24, R2=0.88, Rc2=0.21
1981-1999: Y=-0.015X+0.21, R2=0.76, Rc2=0.33
2000-2011: Y=-0.017X-0.022, R2=0.93, Rc2=0.50
Wind speed anomaly: m s-1
Time: Year
(f) Spring
MK1
MK2
95% level
Time: Year
(c) Summer
SWS_Summer
Low-pass filter
Linear trend_1981-2011
Linear trend_1981-1999
Linear trend_2000-2011
1981-2011: Y=-0.009X+0.15, R2=0.75, Rc2=0.21
1981-1999: Y=-0.0085X+0.14, R2=0.39, Rc2=0.33
2000-2011: Y=-0.014X-0.003, R2=0.78, Rc2=0.50
Wind speed anomaly: m s-1
Time: Year
(g) Summer
MK1
MK2
95% level
Time: Year
(d) Autumn
SWS_Autumn
Low-pass filter
Linear trend_1981-2011
Linear trend_1981-1999
Linear trend_2000-2011
1981-2011: Y=-0.012X+0.19, R2=0.70, Rc2=0.21
1981-1999: Y=-0.008X+0.15, R2=0.24, Rc2=0.33
2000-2011: Y=-0.016X-0.022, R2=0.60, Rc2=0.50
Wind speed anomaly: m s-1
Time: Year
(h) Autumn
MK1
MK2
95% level
Time: Year

Table 1 Comparing wind speed trends calculated using the least-square method (LSM) vs. those calculated using the Theil-Sen approach (TSA). (unit: m s^{-1} a^{-1})

	1981–1999		2000–2011		1981–2011	
	LSM slope	TSA slope	LSM slope	TSA slope	LSM slope	TSA slope
Winter	−0.011*	−0.011	0.00008	0.00014	−0.009*	−0.009
Spring	−0.015*	−0.014	−0.017*	−0.017	−0.014*	−0.013
Summer	−0.0085*	−0.0067	−0.014*	−0.014	−0.009*	−0.009
Autumn	−0.008	−0.007	−0.016*	−0.0158	−0.012*	−0.011

The asterisk denotes the linear trend computed by LSM can pass the significant *t* test at the 99% confidence level

influence of auto-correlation of time series on the Mann-Kendall test is evident, but the increasing trend of SWS in winter since 2000 can be observed based on MK1 and MK2. Therefore, in accordance with the linear fitting, TSA slope, and the Mann-Kendall test (including MK1 and MK2), the rise of the winter SWS during the period of 2000–2011 was not significant at the 90% level, but this recovery of SWS during winter occurred after a long-term decrease before 2000. These specific changes were not consistent with other three seasons, and reasons of the recovery in SWS during winter since 2000 should be intensively explored. Therefore, the spatio-temporal characteristics of SWS during winter and the potential causes will be further investigated in the following parts.

3.2 Spatio-temporal changes of SWS during winter

In order to further investigate a possible recovery of SWS occurred during winter, the principal component analysis (PCA), also known as the empirical orthogonal function (EOF) analysis, was also used to analyze the spatio-temporal characteristics of the winter SWS during the period 1981–2011 (Fig. 3). The first two modes and the corresponding principal components (PCs) could explain approximately 26.7 and 14.9% of the total variances, and both the first two modes were significant at the 95% level according to the North test. The spatial characteristics in the first and second EOF modes are shown in Fig. 3a, b, and their temporal

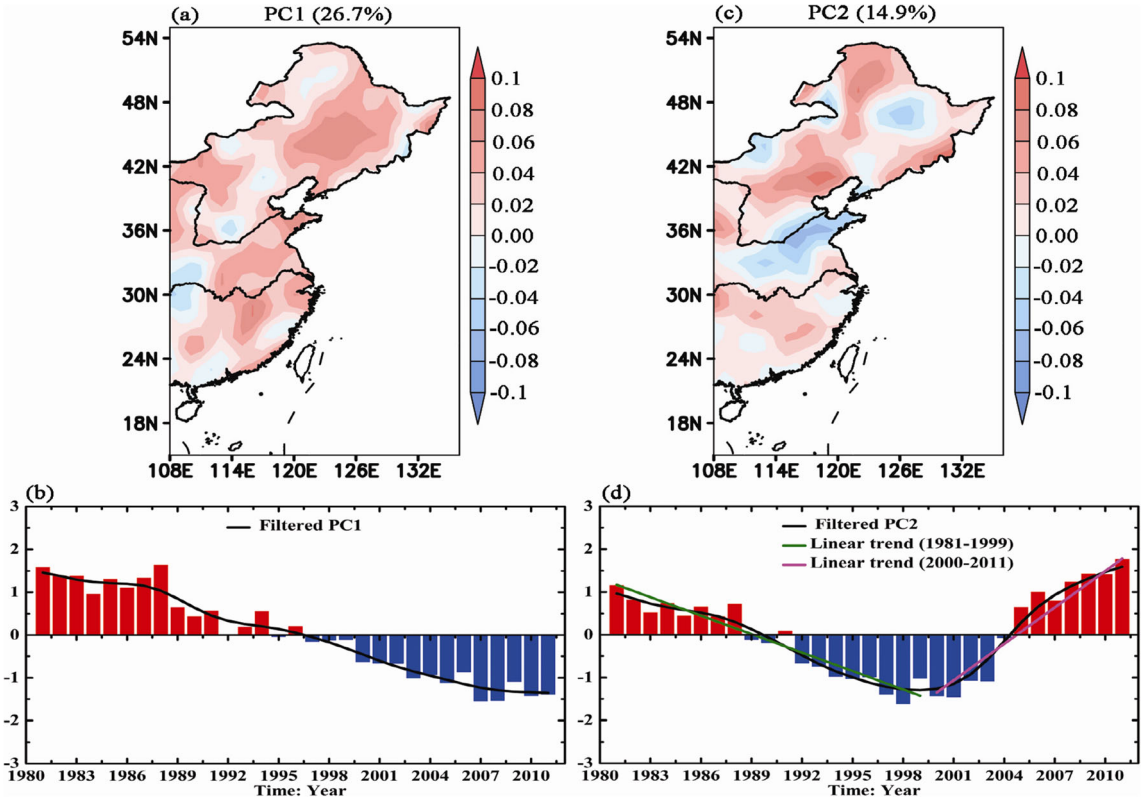

Fig. 3 Principal component analysis (PCA) of the SWS in winter during the period 1981–2011. **a**, **c** The first and second mode, respectively. **b**, **d** Their respective time series. The first and second mode passed the significant North test. (The black lines in **b**, **d** denote the 9-year low-pass-filtered time series with a Gaussian-type filter, and the green and pink lines in **d** denote linear trend of PC2 between 1981–1999 and 2000–2011, respectively)

changes, namely the principal components (PC1, PC2), are presented in Fig. 3c, d. The EOF1 was characterized by a positive pattern covering the whole Eastern China; meanwhile, the PC1 presented a long-term decreasing trend. The PC1 and the EOF1 of the SWS indicated a whole reduction of the SWS from 1981 to 2011 in Eastern China, which was also revealed by the SWS dataset itself (Fig. 2a). Meanwhile, the EOF2 was characterized by a negative pattern covering the middle region of Northeastern China and the basin between the Yellow River and the Huai River, as well as the Shandong Peninsula, and a positive pattern was revealed in other regions in Eastern China; at the same time, the PC2 showed a decreasing trend before 2000, followed by an increasing trend after 2000. Combined the spatio-temporal characteristics in Fig. 3c, d, it could be concluded that a rise in the SWS appeared in most regions over Eastern China since 2000, except a decreasing trend in the middle region of Northeastern China and the basin between the Yellow River and the Huai River, as well as the Shandong Peninsula. This means that a possible recovery of SWS during winter revealed by Fig. 2a occurred in most but not all regions in Eastern China, which should account for the fact that the recovery failed to pass the significant *t* test and the Mann-Kendall test at 95% confidence level. At the same time, the recovery of the SWS during winter revealed by Fig. 2a was embodied in the second mode and the PC2 with the beginning point at the year of 2000, by contrast the unique long-term lasting decreasing trend reflected by the first mode and the PC1. Therefore, the PCA also revealed a recovery of SWS during winter since 2000.

According to the abovementioned results, the SWS during winter in the whole study period was divided into two periods by the turning point 2000, and a comparison of the averaged SWS between the two periods of 1981–1999 and 2000–2011, as well as their difference, is shown in Fig. 4. The main spatial patterns of SWS in the two periods were same, in which larger SWS was found in Northern and Northeastern China and onshore regions in Eastern and Southeastern China. In addition, the mean SWS during 2000–2011 was significantly smaller than that during 1981–1999 in most areas of Northern and Northeastern China for 0.1–0.4 m s^{-1}, and at the same time, some regions appeared to have larger SWS during 2000–2011 than before, such as the southern part of Northern China, the northern part of Northeastern China, and the middle region of China, in which the maximum difference reached 0.3 m s^{-1} (Fig. 4c). Despite a possible recovery in SWS occurred since 2000, the significantly previous decrease during 1981–1999 also predicted the negative difference of the latter period relative to the former in most areas in Eastern China, and most stations with negative SWS bias could pass the significant *t* test at 90% level as shown by Fig. 4c.

The linear trends of SWS during 1981–1999 and 2000–2011 are compared in Fig. 5. A significant decreasing trend was found in many areas in Eastern China except the lower reaches of the Yellow River (Fig. 5a). During the period 1981–1999, the decrease (increase) in SWS was observed in 228 (100) stations, which accounted for 70% (30%) of the total stations. Furthermore, 146 stations showing decreasing trends of SWS passed the significant *t* test at the 90% confidence level, which accounted for the 64% of the stations that showed downward trends. The averaged decreasing trend of 146 stations was −0.31 m s^{-1} $decade^{-1}$. In addition, 45 stations showing increasing trends of SWS passed the significant *t* test at the 90% confidence level, which accounted for 45% of the stations that showed upward trends. The average linear trend coefficients reached −0.11 m s^{-1} $decade^{-1}$ for 1981–1999 in whole Eastern China region, and the most distinct decreasing trend was revealed in

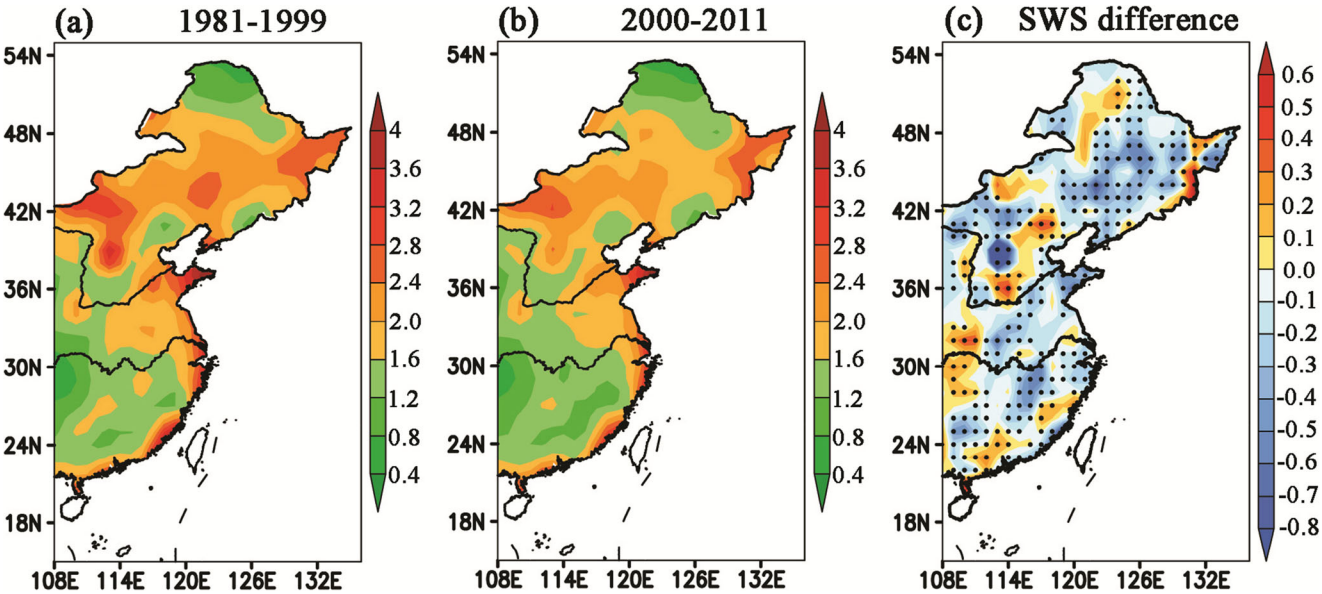

Fig. 4 Spatial patterns of the averaged SWS (unit: m s^{-1}) in winter during the two periods: 1981–1999 (**a**) and 2000–2011 (**b**) and their difference (**c**). (The black dots in **c** denote the trend coefficients passed the significant *t* test at 90% confidence level)

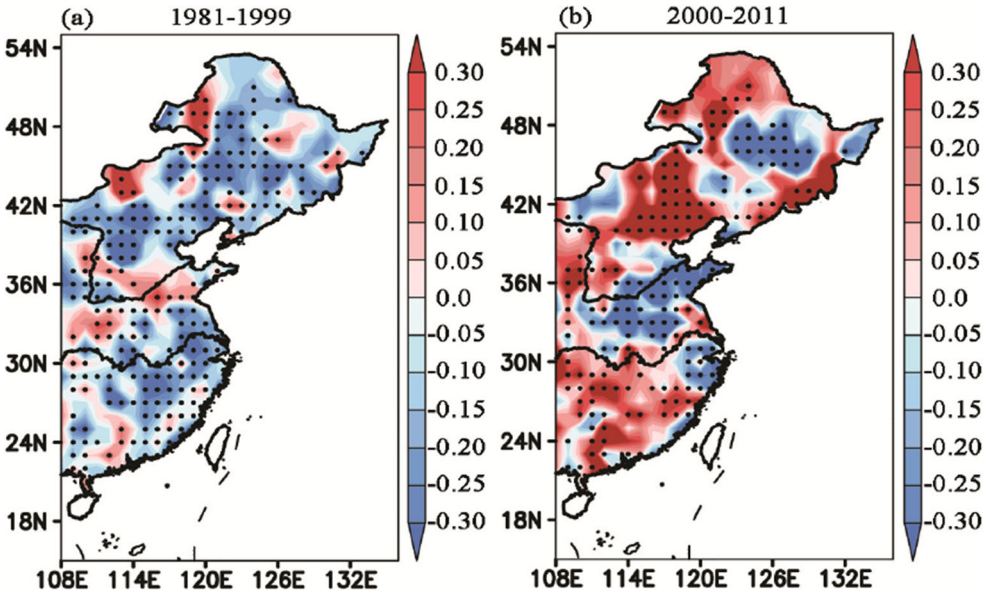

Fig. 5 Spatial patterns of the linear trend coefficients of SWS (unit: m s^{-1} $decade^{-1}$) in winter during the two periods: 1981–1999 (**a**) and 2000–2011 (**b**). (The black dots in **a**, **b** denote the trend coefficients passed the significant *t* test at the 90% confidence level)

the lower reaches of the Yangtze River and in Northern China at a rate of − 0.3 m s^{-1} $decade^{-1}$.

On the contrary, a different pattern of the linear trend coefficients was exhibited after 2000 in the study region (Fig. 5b). An increasing trend could be observed in most areas, including southern and northern parts of Northeastern China, Northern China, and southern region to the Yangtze River, in which the largest trend coefficient reached 0.3 m s^{-1} $decade^{-1}$, which passed the significant *t* test at the 90% confidence level. Furthermore, a decreasing trend was presented in the middle region of Northeastern China, the Shandong Peninsula, the basin between the Yellow River and the Huai River, and regions to the south of the Yangtze River delta region. During the period 2000–2011, the average trend coefficient of SWS reached 0.0008 m s^{-1} $decade^{-1}$ in whole Eastern China. Furthermore, 164 stations showed reduction of SWS, and 164 stations showed an increase of SWS, which accounted for 50% of total stations, respectively. Therefore, the stations that showed increasing (decreasing) trends increased (decreased) by 20% with respect to the period of 1981–1999. Moreover, 82 stations showing decreasing trend of SWS passed the significant *t* test at the 90% confidence level, which accounted for 50% of the stations that showed the downward trends, and 95 stations showing increasing trends of SWS passed the significant *t* test at the 90% confidence level, which accounted for the 58% of the stations showing upward trends. The averaged increasing trend of 95 stations was 0.50 m s^{-1} $decade^{-1}$. Therefore, with respect to the period 1981–1999, the stations showing significant increasing trends increased 45%, and the stations showing significant decreasing trends decreased 44%.

3.3 Causes of the recovery in the SWS

From the dynamics perspective, the motion in the atmosphere should obey the Navier-Stokes dynamical equation, in which both the driving force and drag force can take effects on atmospheric motion (Wu et al. 2017b). Therefore, the causes of wind speed change should be analyzed from the view of changes in drag and driving force of air motion. The PGF is the driving force, which is the most important factor causing air motion, and the role of the PGF in the long-term changes of SWS has been revealed in the previous studies (Klink 1999a; Tuller 2004). At the same time, some studies also used the air pressure difference between different latitudes and geostrophic wind at 850 hPa to evaluate the effects of the driving force on the SWS at different regions (You et al. 2010; Guo et al. 2011; Lin et al. 2013). Furthermore, some quantitative results about the effects of PGF on SWS have also been reported (Klink 1999b, 2007; Clifton and Lundquist 2012). In recent, a reduction in the annual mean PGF from the near-surface layer to 300 hPa was also found in Eastern China during 1980–2011, and the decrease of PGF was similar to the slowdown of SWS. Furthermore, a quantitative evaluation about the influence of the PGF on the changes of annual mean SWS in different regions also presented that the PGF was a important factor affecting the change of SWS (Wu et al. 2017b). The drag force involves the changes of surface roughness induced by the LUCC (Wu et al. 2017b, c). Some previous studies have revealed that the surface roughness should be an increasing trend in Eastern China induced by LUCC in recent 30 years due to the occurrence of large-scale urbanization and the policy of returning farming to tree planting exerted from 1999 (Liu and Tian 2010; Asselen and Verburg 2013; Liu et al. 2014); therefore, the surface roughness could hardly

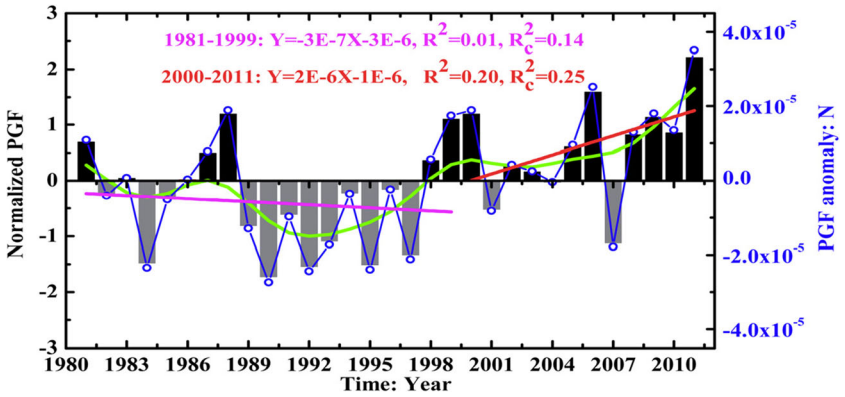

Fig. 6 Temporal changes of the pressure-gradient force in winter during the period of 1981–2011. (The bar denotes the normalized PGF, and the blue line denotes the PGF anomaly. The green line denotes the 9-year low-pass-filtered time series by a Gaussian-type filter. The pink and red lines denote the linear fitting during the periods 1981–1999 and 2000–2011, respectively. R is the correlation coefficient, R_c is the threshold of significant t test at the 90% confidence level)

be shifted from an increase to a decrease, which means that the possible recovery in SWS since 2000 could not be explained using the reduction of surface roughness. Hence, the change of PGF before and after 2000 should be analyzed.

Temporal changes of the PGF from 1981 to 2011 in Eastern China are shown in Fig. 6, in which a negative anomaly during 1981–1998 was presented by the 9-year low-pass-filtered PGF data associated by a positive anomaly during 1999–2011. From 1981 to 1999, the positive PGF years accounted for 31.6% of total years, which reached 83.3% during 2000–2011. This result meant that the PGF became stronger after 1999 than before. In addition, the average linear trend coefficient of PGF was -3.0×10^{-6} and 2.0×10^{-5} N decade^{-1} for the periods of 1981–1999 and 2000–2011, respectively. Though the linear trend coefficients failed to pass the significant t test at the 90% confidence level, the increasing trend since 2000 was more significant than the decreasing trend before 2000. Furthermore, the correlation coefficient between PGF and SWS reached 0.7 after 2000, which passed the significant t test at the 99% confidence level. Therefore, the fact of increase in PGF from 2000 to 2011 was in accordance with the possible recovery of SWS in the same period revealed by Fig. 2a.

Spatial patterns of the PGF in winter during the two periods of 1981–1999 and 2000–2011 as well as their difference are shown in Fig. 7. The average PGF during 1981–1999 presented a pattern of big value in northern part and uniform distribution in other regions, in which the value of PGF lay between 3×10^{-4} and 4×10^{-4} N in most regions in Eastern China. The pattern of PGF during 2000–2011 differed from that during 1981–1999 in the following three aspects: the maximum value in the northern part of Northeastern China disappeared; the region with large PGF between 6×10^{-4} and 8×10^{-4} N in Northern China extended

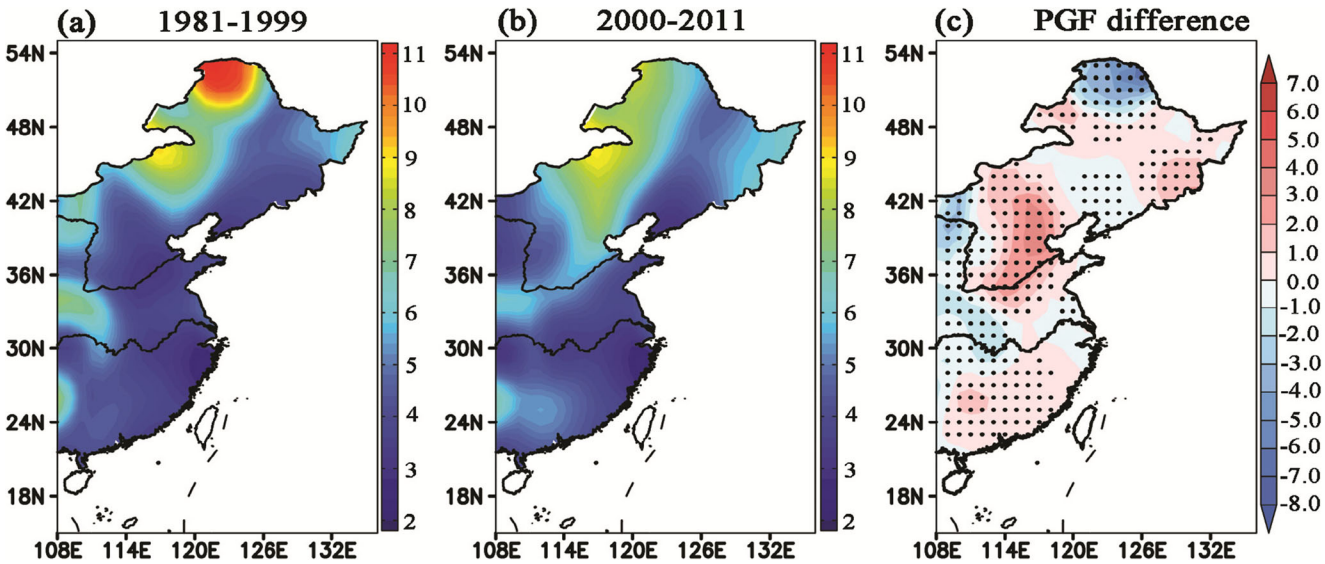

Fig. 7 Spatial patterns of the pressure-gradient force (unit: 10^{-4} N) in winter during the two periods of 1981–1999 (**a**) and 2000–2011 (**b**), as well as the PGF difference between 1981–1999 and 2000–2011 (**c**). (The black dots in **c** denote the trend coefficients passed the significant t test at 90% confidence level)

southerly to the low reaches of the Yellow River; and the region with large PGF between 5×10^{-4} and 7×10^{-4} N in the southwest of the research domain spread easterly into Southern China. In general, the value of PGF fell between 5×10^{-4} and 6×10^{-4} N in most areas, which was larger than that during 1981–1999. The difference of PGF between the two periods was positive in many areas in study region with the mean value of 2.22×10^{-5} N; meanwhile, the maximum difference 5×10^{-4} N was found in Northern China. At the same time, the difference of PGF showed a statistical significance exceeding 90% level in most stations in Eastern China. In addition, a negative difference in PGF between the two periods could be observed in the middle area of Northeastern China and the basin between the Yellow River and the Huai River, as well as the region in southern part of the Yangtze River delta region, which meant a decrease in PGF in these regions during 2000–2011 relative to 1981–1999. These regions with decreasing PGF were similar to the spatial characteristics of linear trend coefficient in the SWS as shown by Fig. 5b.

The linear trend coefficients of the PGF were positive in Southern China, Northern China, and eastern part of Northeastern China during 1981–1999 (Fig. 8a), and negative linear trend coefficients were found in other regions. A statistically significant decreasing trend could be found in the middle and lower reaches of Yangtze River and the middle and northern region of Northeastern China during 1981–1999, which was in accordance with the linear trend coefficients of SWS (Fig. 5a). At the same time, a statistically significant increasing trend in Northern China during 1981–1999 (Fig. 8a) was presented, which was corresponding to a distinct decreasing trend in the SWS (Fig. 5a). Similar inconformity in spatial distribution of temporal tendencies between SWS and PGF was formerly reported in Southeastern China (Wu et al. 2016), and the main cause was attributed to the rise of surface roughness led by LUCC in recent years. Northern China was one of the most developed city cluster in China, in which wide urbanization happened in recent 30 years; therefore, the inconformity between the changes in SWS and PGF during 1981–1999 should also be explained by the rise of surface roughness attributed to LUCC in this region.

Distinct increasing trend in PGF during the period 2000–2011 was revealed in many regions in Eastern China, except for the eastern part of Northeastern China and Northern China, as well as the middle region of China (Fig. 8b). The increase in PGF in Northern and Southern China from 2000 to 2011 was in accordance with the linear trends of SWS in these regions, which meant that the PGF was the main cause inducing the recovery of the SWS in these regions. An inconformity in spatial distribution between SWS and PGF for the period 2000–2011 could also be observed in the regions with decreasing SWS shown by Fig. 5b, which included the middle area of Northeastern China and the basin between the Yellow River and the Huai River, as well as the southern part of the Yangtze River delta region. The cause of the fact that a rise of PGF could not lead to an increase in SWS could be caused by a rise of drag force attributed to an increase in surface roughness, which could offset the increase in the driving force. In addition, a significant rise of the PGF during 2000–2011 could be found in most stations, which accounted for the general increase in SWS during this period.

4 Discussion

4.1 Potential cause of the rise in the PGF since 2000

The PGF is the driving force of air motion, which was caused by the horizontal difference in air pressure, so the reason inducing the increase of PGF during the period 2000–2011 should be

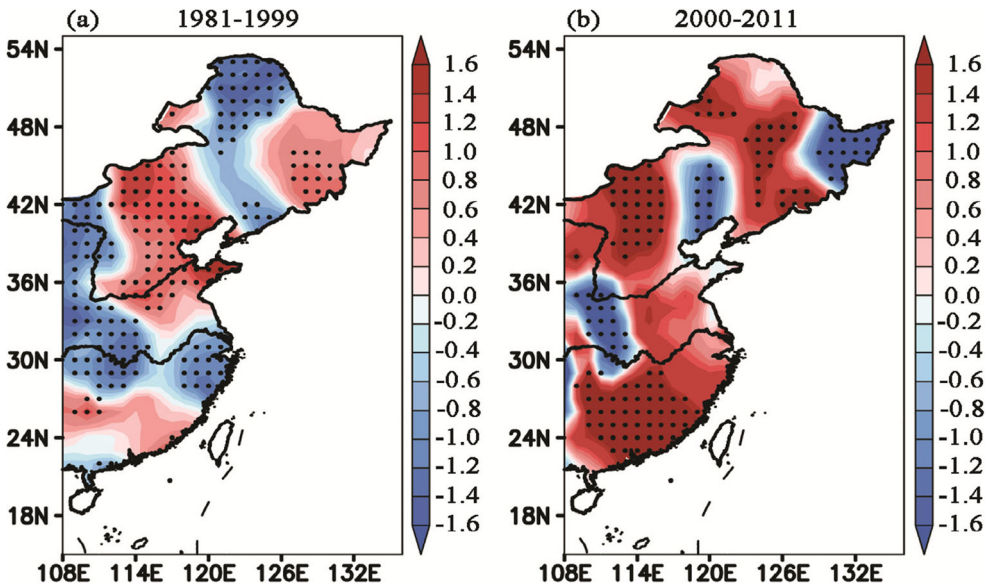

Fig. 8 Spatial patterns of the linear trend coefficients of the normalized pressure-gradient force (unit: decade^{-1}) in winter during the two periods of 1981–1999 (**a**) and 2000–2011 (**b**). (The black dots in **a**, **b** denote the trend coefficients passed the significant *t* test at 90% confidence level)

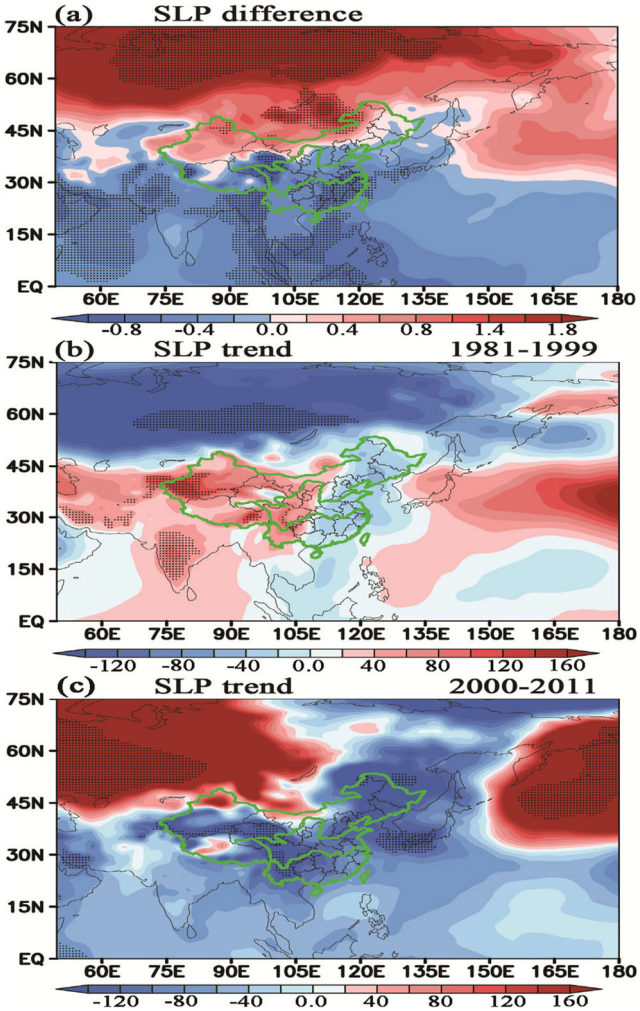

Fig. 9 Spatial patterns of the ERA-Interim sea-level pressure (SLP) difference (unit: hPa) between 1981–1999 and 2000–2011 (**a**) and the linear trends of SLP during the two periods of 1981–1999 (**b**) and 2000–2011 (**c**) (unit: Pa decade^{-1}). (The black dots denote the region passed significant *t* test at 90% confidence level)

searched in the change of SLP. Spatial pattern of the SLP difference between 1981–1999 and 2000–2011 is shown in Fig. 9a. A notable increase in SLP was observed in the belt between 45° N and 75° N, in which the increase of SLP could exceed 1.4 hPa with the maximum of 1.8 hPa ($p < 0.10$ level). In addition, the statistically significant difference of SLP occurred in the region of the Siberian high. On the other hand, a distinct decrease was observed between 0°–30° N, in which the SLP difference exceeded 0.4 hPa with the maximum of 1.0 hPa ($p < 0.10$ level). A statistically significant difference was revealed in the Arabian Sea, the Bay of Bengal, and the South China Sea. These results implied that a significant shift in the mean SLP before and after 2000 was revealed, which amplified the longitudinal difference of PGF. It should be noted that the study region was located between the two belts with significant difference of SLP; therefore, the change of longitudinal PGF could evidently affect the SWS in Eastern China.

Changes of the mean SLP during the two periods were further analyzed, and the results are shown in Fig. 9b, c. The temporal changes of SLP from 1981 to 1999 showed a pattern of "increase in south and decrease in north," which meant a significant decreasing trend between 45° N and 75° N associated an increasing trend to the south of 45° N. A reverse pattern of "decrease in south and increase in north" was revealed during the period 2000–2011. These results indicated that a transition from a decrease to an increase in SLP happened close to 2000 between 45° N and 75° N, and at the same time, an opposite transition from an increase to a decrease also occurred in the regions to the south of 45° N; therefore, a transition in the PGF occurred in the year 2000. These characteristics, combined with the lasting decreasing trend of SLP during 2000–2011 in Eastern China, amplified the SLP difference between Eastern China and northern region of the research domain, which should account for the rise in the PGF in Eastern China.

In order to investigate the relationship between the PGF in Eastern China and the SLP, the correlation coefficient was calculated. The pattern of correlation coefficient between PGF in Eastern China and SLP in Asia region is shown in Fig. 10, in which positive and negative correlation coefficients were revealed in northern part of Asia and in southern and eastern part of Asia, respectively. The averaged correlation coefficient in the region (51° N–69.75° N; 51.75° E–111.75° E) (represented by subregion hereafter) exceeded 0.6, which passed the significant *t* test at 99% level. Furthermore, the negative correlation coefficient in the southern part of the research domain failed to pass the significant *t* test at the 99% confidence level. Therefore, the results indicated that the relationship between SLP in the subregion and PGF in the Eastern China was significant, and at the same time, the changes of PGF in Eastern China were consistent in phases with the SLP in the subregion.

Temporal changes of the SLP anomaly in the subregion during the period 1981–2011 are shown in Fig. 11a. A reduction in SLP was revealed during 1981–1999 at a decreasing

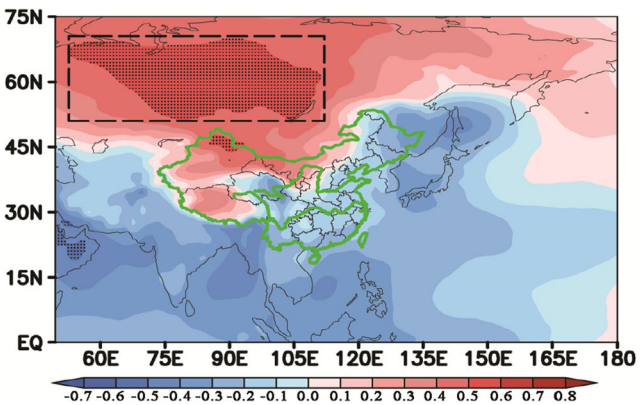

Fig. 10 The spatial pattern of correlation coefficients between pressure-gradient force (PGF) in Eastern China and SLP. (The dashed rectangle denotes the subregion: 51° N–69.75° N; 51.75° E–111.75° E. The black dots represent the correlation coefficient passed the significant *t* test at 99% confidence level)

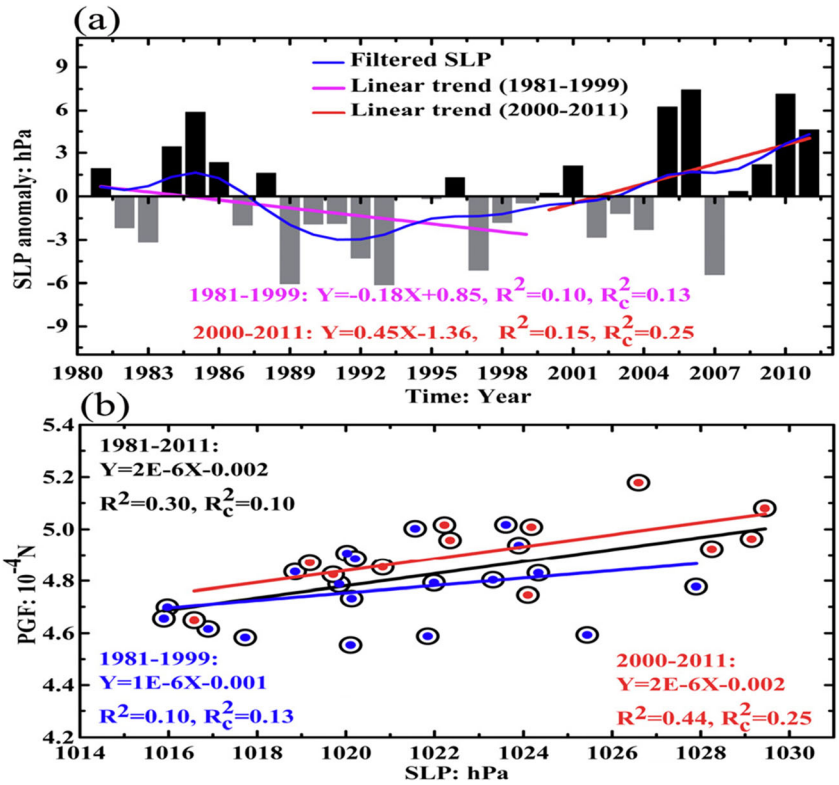

Fig. 11 Temporal changes of SLP anomaly in the subregion (51° N–69.75° N; 51.75° E–111.75° E) during the period of 1981–2011 (**a**) and the regression between the PGF in Eastern China and the SLP in the subregion (**b**). (In **a**, the blue line denotes the 9-year low-pass-filtered time series by a Gaussian-type filter; the pink and red lines denote the linear fitting of SLP during the periods 1981–1999 and 2000–2011, respectively. In **b**, the black circles, blue dots, and red dots denote the periods of 1981–2011, 1981–1999, and 2000–2011, respectively; the black, blue, and red lines denote the linear fitting during the periods of 1981–2011, 1981–1999, and 2000–2011, respectively. In addition, R is the correlation coefficient, and R_c is the threshold of the significant t test at 90% confidence level)

trend of − 1.8 hPa decade^{-1} ($p > 0.10$ level), followed by an increase in SLP since 2000 at an increasing trend of 4.5 hPa decade^{-1} ($p > 0.10$ level). Therefore, the temporal changes of SLP during the two periods were similar to the temporal changes of PGF as shown in Fig. 6. Furthermore, the probability of the same sign of the anomaly appearing at the same time (PAST) between the PGF in Eastern China and the SLP in the subregion reached 68% during the period 1981–2011, which increased to 75% during the period 2000–2011. The positive SLP anomaly years accounted for 31.6% of total years during the period 1981–1999, which increased to 66.7% since 2000. These results indicated that the SLP should be stronger during the period 2000–2011 than that during the whole study period. In addition, the linear regression between the PGF in Eastern China and SLP in subregion showed positive correlation during different periods (Fig. 11b). The regression coefficient during 1981–1999 failed to pass the significant t test at 90% level, which was statistically significant at 90% level for the periods of 1981–2011 and 2000–2011. At the same time, the largest correlation coefficient 0.66 appeared during 2000–2011, which passed the significant t test at the 90% confidence level. These results meant that the increase of SLP in the subregion played more important role in the rise of PGF in Eastern China after 2000 than before.

4.2 Monthly changes of SLP in the subregion

Monthly changes of SLP in the subregion between the two periods of 1981–1999 and 2000–2011 are summarized in Fig. 12. The SLP generally showed decreasing trends in December, January, and February from 1981 to 1999, in which the linear trend coefficients passed the significant t test at 90% confidence level in few areas in December and in most regions to the west of 75° E in February. There were many regions showing an increasing trend in the SLP in December, January, and February since 2000, in which the linear trend coefficients passed the significant t test at 90% level in nearly all the subregion in January and in a few areas in northwestern subregion in February. These spatial characteristics indicated that the rise of SLP in the subregion mainly occurred in January and February since 2000, which predominated in the rise of the PGF in winter in Eastern China after 2000. The temporal changes of SLP in December, January, and February are shown in Fig. 13. The results showed that the SLP in the subregion presented a downward trend in December, January, and February during 1981–1999, and the decreasing trend in February passed the significant t test at 90% level (Fig. 13c). The SLP in the subregion showed a downward trend in December during 2000–2011, which failed to pass the significant t test at 90% level (Fig. 13a). However, the SLP in January showed a significant increase at a rate of 9.1 hPa decade^{-1} ($p < 0.01$ level) after 2000 (Fig. 13b). In February, a weak increase in SLP was also observed, with the increasing trend of 3.9 hPa decade^{-1}, which failed to pass the significant t test at the 90% confidence level (Fig. 13c). In addition, the 9-year low-pass-filtered curves in December, January, and February presented similar transition from decrease to increase close to the year of 2000, which

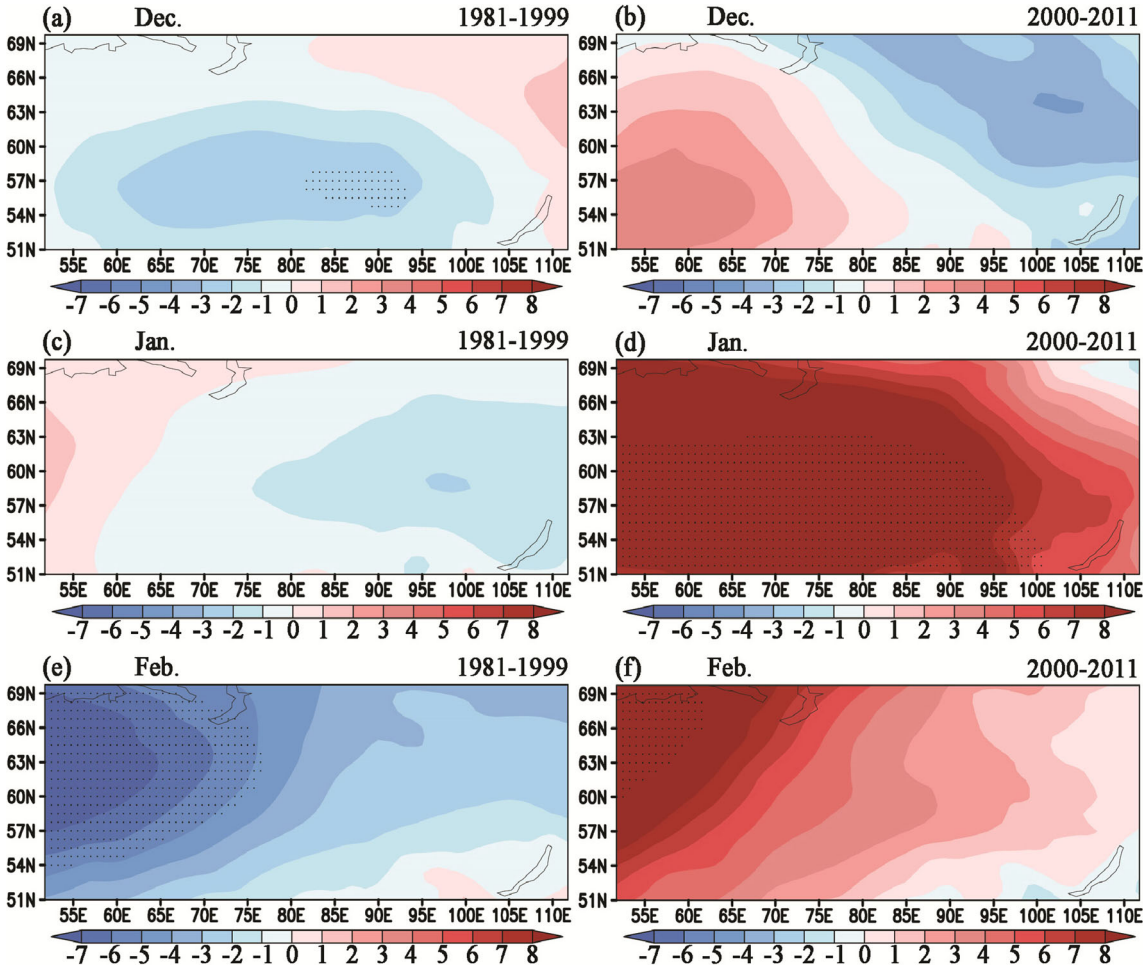

Fig. 12 Spatial patterns of linear trend of SLP in the subregion (51° N–69.75° N; 51.75° E–111.75° E) (unit: hPa decade^{-1}) during the two periods of 1981–1999 (**a**, **c**, **e**) and 2000–2011 (**b**, **d**, **f**). (**a**, **b** December. **c**, **d** January. **e**, **f** February. The black dots denote linear trend coefficients passed the significant *t* test at 90% confidence level)

arranged proof for the turning in the SLP in adjacent regions of Eastern China and in the PGF in Eastern China.

5 Conclusion

In this paper, an analysis of the long-term changes in SWS over Eastern China was carried out, and a weak recovery in the winter SWS was revealed during 2000–2011 after the lasting decrease since 1981. After that, an analysis about the cause inducing the SWS recovery was implemented from the view of the driving force. The main results can be summarized as the following:

(1) The SWS showed a downward trend in the last 30 years, and at the same time, the strongest decreasing trend was observed during spring (-0.14 m s^{-1} decade^{-1}; $p < 0.01$ level), and the weakest decreasing trend was observed during winter and summer (-0.09 m s^{-1} decade^{-1}; $p < 0.01$ level). Since 2000, the SWS showed a downward trend during spring, summer, and autumn, with a decreasing rate of -0.17, -0.14, and -0.16 m s^{-1} decade^{-1}, respectively. A weak increasing rate of 0.0008 and 0.00136 m s^{-1} decade^{-1} during winter was found from 2000 to 2011 based on LSM and non-parametric TSA, respectively, though this increasing rate failed to pass the significant *t* test at 99% level. Therefore, the change of SWS during winter since 2000 was not consistent with other three seasons, and a short-term strengthening of winter SWS occurred since 2000.

(2) A possible recovery of the SWS after 2000 was revealed by linear fitting, non-parametric TSA slope, the Mann-Kendall test (including MK1 and MK2), and the PCA, and at the same time, this was embodied in the second principal component of SWS. Furthermore, a possible recovery of SWS since 2000 was mainly induced by the changes of PGF over Eastern China, which could be attributed to the changes of SLP in the region: 51°–69.75° N; 51.75°–111.75° E. The long-term changes of the PGF in Eastern China during the two periods of 1981–1999 and 2000–2011 were significantly related to the change of SLP in the abovementioned

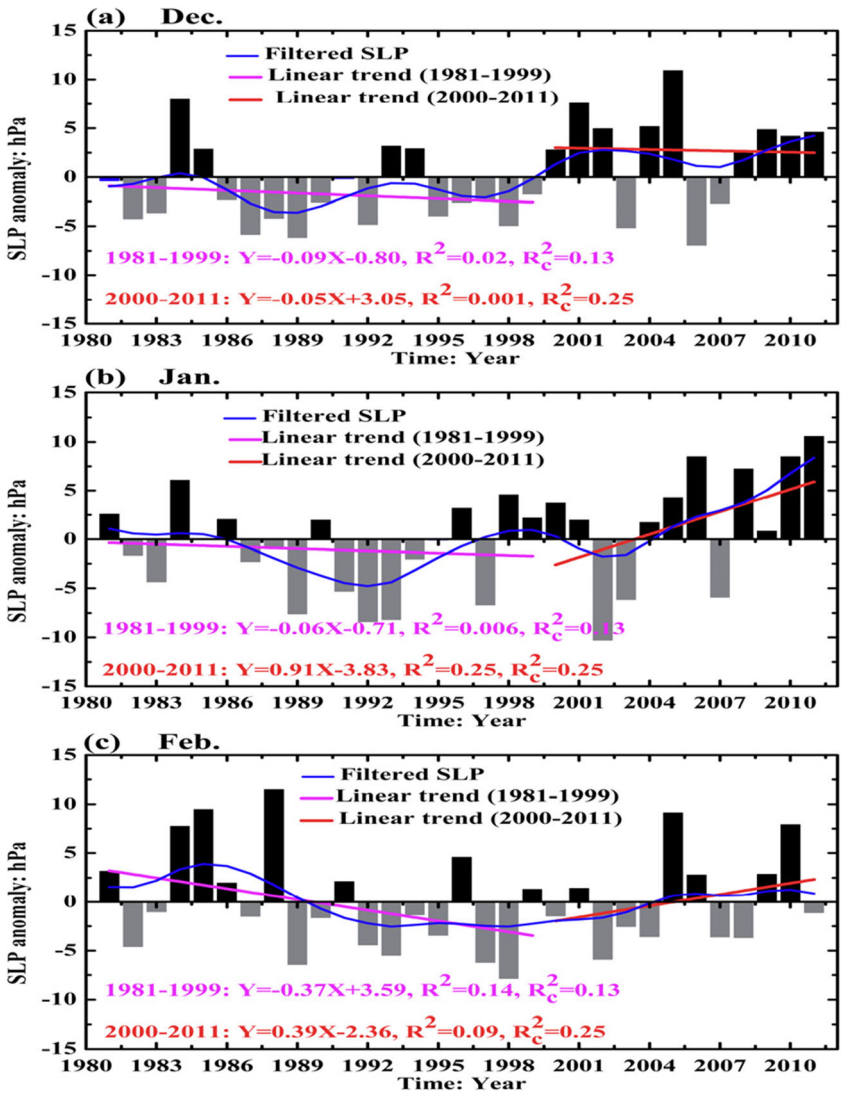

Fig. 13 Temporal changes of SLP anomaly in the subregion (51° N–69.75° N; 51.75° E–111.75° E) in December, January, and February. (The blue lines denote the 9-year low-pass-filtered time series by a Gaussian-type filter. The pink and red lines denote the linear trend of SLP during 1981–1999 and 2000–2011, respectively. *R* is the correlation coefficient, and *R*c is the threshold of the significant *t* test at 90% confidence level)

region. Furthermore, the increase in SLP during winter in the subregion was mainly observed in January, with the increasing trend of 0.91 hPa decade^{-1}, which passed the significant *t* test at the 90% level.

In this study, a possible recovery of SWS during winter in Eastern China since 2000 has been revealed and analyzed using the station observed SWS dataset and ERA-Interim SLP reanalysis dataset. The potential reasons causing the recovery of SWS have been attributed to the rise of PGF based on the statistical analysis, which was induced by the changes of SLP in adjacent regions. Therefore, the short-term strengthening of SWS presented in this paper may help promote future studies in this direction. However, a quantitative evaluation for the different roles for the driving force and the drag force on the observed recovery in the SWS is still absent, which is a shortcoming for much deep comprehension about the SWS recovery in Eastern China. In recent decades, distinct LUCC in China have made the increase in surface roughness in many regions; therefore, this means a uniform rise in the PGF could lead to different recovery of SWS in different regions, which should be carefully evaluated using the credible numerical models in future.

Acknowledgements The authors cordially thank the reviewers for their thorough comments and constructive suggestions, which improve the paper quality significantly. Daily meteorological data is available from the China Meteorological Data Sharing Service System, and the ERA-Interim dataset comes from the ECMWF. We thank all the dataset providers. This study was sponsored by the Chinese Natural Science Foundation (41675149, 41775087), the National Key Research and Development Program of China (2016YFA0600403), and the Yunnan Province Education Department Project (2017YJS106). The paper was also supported by the Program for Key Laboratory in University of Yunnan Province, the Chinese Jiangsu Collaborative Innovation Center for Climate Change, and the Young Scholar of Distinction for Doctoral Candidate of Yunnan Province in 2016.

References

Asselen SV, Verburg PH (2013) Land cover change or land-use intensification: simulating land system change with a global-scale land change model. Glob Chang Biol 19:3648–3667

Aziz OIA, Burn DH (2006) Trends and variability in the hydrological regime of the Machenzie River basin. J Hydrol 319(1–4):282–294

Azorin-Molina C, Vicente-Serrano SM, McVicar TR, Jerez S, Sanchez-Lornzo A, Lopez-Moreno JI, Revuelto J, Trigo RM, Lopez-Bustins JA, Espirito-Santo F (2014) Homogenization and assessment of observed near-surface wind speed trends over Spain and Portugal, 1961-2011. J Clim 27:3692–3712

Azorin-Molina C, Guijarro JA, McVicar TR, Vicente-Serrano SM, Chen DL, Jerez S, Espirito-Santo F (2016) Trends of daily peak wind gusts in Spain and Portugal, 1961-2014. J Geophys Res-Atmos 121:1059–1078. https://doi.org/10.1002/2015JD024485

Bandyopadhyay A, Bhadra A, Raghuwanshi NS, Singh R (2009) Temporal trends in estimates of reference evapotranspiration over India. J Hydrol Eng 14(14):508–515

Berrisford P, Tobin I, Dunn RJH, Vautard R, McVicar TR (2015) [Global climate; atmospheric circulation; surface winds] land surface wind speed [in "State of the climate in 2014"]. Bull Am Meteorol Soc 95(7):S33–S34

Bichet A, Wild M, Folini D, Schar C (2012) Causes for decadal variations of speed over land: sensitivity studies with a global climate model. Geophys Res Lett 39:L11701. https://doi.org/10.1029/2012GL051685

Birsan MV, Molnar P, Burlando P, Pfaundler M (2005) Streamflow trends in Switzerland. J Hydrol 314(1–4):312–329

China Meteorological Administration (CMA) (2003) Ground surface meteorological observation. China Meteorological Press, Beijing, p 157

Clifton A, Lundquist JK (2012) Data clustering reveals climate impacts on local wind phenomena. J Appl Meteorol Climatol 51:1547–1557

Cressman GP (1959) An operational objective analysis system. Mon Weather Rev 87:367–374

Cusack S (2013) A 101 year record of windstorms in the Netherlands. Clim Chang 116:693–704. https://doi.org/10.1007/s10584-012-0527-0

Dadaser-Celik F, Cengiz E (2014) Wind speed trends over Turkey from 1975 to 2006. Int J Climatol 34:1913–1927. https://doi.org/10.1002/joc/3810

Dee DP, Uppala SM, Simmons AJ, Berrisford P, Poli P, Kobayashi S, Andrae U, Balmaseda MA, Balsamo G, Bauer P, Bechtold P, Beljaars ACM, van de Berg L, Bidlot J, Bormann N, Delsol C, Dragani R, Fuentes M, Geer AJ, Haimberger L, Healy SB, Hersbach H, Hólm EV, Isaksen L, Kållberg P, Köhler M, Matricardi M, McNally AP, Monge-Sanz BM, Morcrette JJ, Park BK, Peubey C, de Rosnay P, Tavolato C, Thépaut JN, Vitart F (2011) The ERA-Interim reanalysis: configuration and performance of the data assimilation system. Q J R Meteorol Soc 137:553–597. https://doi.org/10.1002/qj.828

Dinpashoh Y (2006) Study of reference crop evapotranspiration in I.R. of Iran. Agric Water Manag 84(1):123–129

Dinpashoh Y, Jhajharia D, Fakheri-Fard A, Singh V, Kahya E (2011) Trends in reference crop evapotranspiration over Iran. J Hydrol 399(3):422–433

Dinpashoh Y, Mirabbasi R, ASCE SM, Jhajharia D, Abianeh HZ, Mostafaeipour A (2014) Effect of short term and long-term persistence on identification of temporal trends. J Hydrol Eng 19(3):617–625

Dunn RJH, Azorin-Molina C, Mears CA, Berrisford P, McVicar TR (2016) Surface winds [in "State of the climate in 2015"]. Bull Am Meteorol Soc 97(8):S38–S40

Fu GB, Yu JJ, Zhang YC, Hu SS, Quyang RL, Liu WB (2011) Temporal variation of wind speed in China for 1961-2007. Theor Appl Climatol 104(3):313–324

Fujibe F (2009) Relation between long-term temperature and wind speed trends at surface observation stations in Japan. SOLA 5:081–084. https://doi.org/10.2151/sola.2009-021

Garcia-Bustamante E, Gonzalez-Rouco JF, Navarro J, Xoplaki E, Jimenez PA, Montavez JP (2012) North Atlantic atmospheric circulation and surface wind in the northeast of the Iberian Peninsula: uncertainty and long term downscaled variability. Clim Dyn 38:141–160. https://doi.org/10.1007/s00382-010-0969-x

Greene JS, Chatelain M, Morrissey M, Stadler S (2012) Estimated changes in wind speed and wind power density over the western High Plains, 1971-2000. Theor Appl Climatol 104(3):313–324. https://doi.org/10.1007/s00704-012-0596-z

Guo H, Xu M, Hu Q (2011) Changes in near-surface wind speed in China: 1969-2005. Int J Climatol 31:349–358. https://doi.org/10.1002/joc.2091

Jiang Y, Luo Y, Zhao ZC, Tao SW (2010) Changes in wind speed over China during 1956-2004. Theor Appl Climatol 99:421–430. https://doi.org/10.1007/s00704-009-0152-7

Jerez S, Trigo RM, Vicente-Serrano SM, Pozo-Vazquez D, Lorente-Plazas R, Lorenzo-Lacruz J, Santos-Alamillos F, Montavez JP (2013) The impact of the North Atlantic oscillation on the renewable energy resources in southwestern Europe. J Appl Meteorol Climatol 52:2204–2225. https://doi.org/10.1175/JAMC-D-12-0257.1

Karnauskas KB, Lundquist JK, Zhang L (2017) Southward shift of the global wind energy resource under high carbon dioxide emissions. Nat Geosci 11:38–43

Kim JC, Paik K (2015) Recent recovery of surface wind speed after decadal decrease: a focus on South Korea. Clim Dyn 45:1699–1712. https://doi.org/10.1007/s00382-015-2546-9

Klink K (1999a) Climatological mean and inter-annual variance of United States surface wind speed, direction and velocity. Int J Climatol 19:471–488

Klink K (1999b) Trends in mean monthly maximum and minimum surface wind speeds in the coterminous United States, 1961 to 1990. Clim Res 13:193–205

Klink K (2007) Atmospheric circulation effects on wind speed variability at turbine height. J Appl Meteorol Climatol 46(4):445–456. https://doi.org/10.1175/JAM2466.1

Kumar S, Merwade V, Kam J, Thurner K (2009) Streamflow trends in Indiana: effects of long term persistence, precipitation and subsurface drains. J Hydrol 374:171–183. https://doi.org/10.1016/j.jhydrol.2009.06.012

Li JP, Wu ZW, Jiang ZH, He JH (2010) Can global warming strengthen the East Asian summer monsoon. J Clim 23:6696–6705. https://doi.org/10.1175/2010JCL13434.1

Li JP, Feng J, Li Y (2011) A possible cause of decreasing summer rainfall in Northeast Australia. Int J Climatol 32(7):995–1005. https://doi.org/10.1002/joc.2328

Lin CG, Yang K, Qin J, Hu Y (2013) Observation coherent trends of surface and upper-air wind speed over China since 1960. J Clim 26:2891–2903

Lin CG, Yang K, Huang JP, Tang WJ, Qin J, Niu XL, Chen YY, Chen DL, Lu N, Fu R (2015) Impacts of wind stilling on solar radiation variability in China. Sci Rep 5(5):15135. https://doi.org/10.1038/srep15135

Liu XN (2000) The homogeity test on mean annual wind speed over China. Quart J Appl Meteorol 11(1):28–34 (in Chinese)

Liu M, Shen YJ, Zeng Y, Liu CM (2010) Trend in pan evaporation and its attribution over the past 50 years in China. J Geogr Sci 20(4):557–568

Liu ML, Tian HQ (2010) China's land cover and land use change from 1700 to 2005: estimations from high-resolution satellite data and historical archives. Global Biogeochemical Cycle 24(3):285–286

Liu Q, McVicar TR (2012) Assessing climate change induced modification of Penman potential evaporation and runoff sensitivity in a large water-limited basin. J Hydrol 464(465):352–362. https://doi.org/10.1016/j.jhydrol.2012.07.032

Liu JY, Kuang WH, Zhang ZX, Xu X, Qin Y, Ning J, Zhou W, Zhang S, Li R, Yan C, Wu S, Shi X, Jiang N, Yu D, Pan X, Chi W (2014) Spatio-temporal characteristics, patterns and causes of land-use changes in China since the late 1980s. J Geogr Sci 24(2):195–210

Mastylo M (2013) Bilinear interpolation theorems and applications. J Funct Anal 265(2):185–207. https://doi.org/10.1016/j.jfa.2013.05.001

McMahon TA, Peel MC, Lowe L, Srikanthan R, McVicar TR (2013) Estimating actual, potential, reference crop and pan evaporation using standard meteorological data: a pragmatic synthesis. Hydrol Earth Syst Sci 17:1331–1363. https://doi.org/10.5194/hessd-10-8781-2013

McVicar TR, Roderick ML, Donohue RJ, Li LT, Van Niel TG, Thomas A, Grieser J, Jhajharia D, Himri Y, Mahowald NM, Mescherskaya AV, Kruger AC, Rehman S, Dinpashoh Y (2012) Global review and synthesis of trends in observed terrestrial near-surface wind speeds: implications for evaporation. J Hydrol 416(417):182–205. https://doi.org/10.1016/j.jhydrol.2011.10.024

Narkhedkar SG, Sinha SK, Mitra AK (2008) Mesoscale objective analysis of daily rainfall with satellite and conventional data over Indian summer monsoon region. Geofizika 25(2):159–178

Novotny EV, Stefan HG (2007) Stream flow in Minnesota: indicator of climate change. J Hydrol 334(3–4):319–333

Pryor SC, Barthelmie RJ, Young DT, Takle ES, Arritt RW, Flory D, Gutowski WJ, Nunes A, Roads J (2009) Wind speed trends over the contiguous United States. J Geophys Res-Atmos 114(D14):1159–1171. https://doi.org/10.1029/2008JD011416

Pryor SC, Ledolter J (2010) Addendum to "Wind speed trends over the contiguous United States". J Geophys Res Atmos 115(D10):1159–1171. https://doi.org/10.1029/2009JD013281

Sen PK (1968) Estimates of the regression coefficients based on Kendall's tau. J Am Stat Assoc 63:1379–1389

Simmons AJ, Uppala S, Dee D, Kobayashi S (2007) ERA-Interim: new ECWMF reanalysis products from 1989 onwards. ECMWF Newsletter 110:25–35

Simmons AJ, Willett KM, Jones PD, Thorne PW, Dee DP (2010) Low-frequency variations in surface atmospheric humility, temperature and precipitation: inferences from reanalysis and monthly gridded observational datasets. J Geophys Res-Atmos 115(D1):1–21. https://doi.org/10.1029/2009JD012442

Simmons AJ, Poli P, Dee DP, Berrisford P, Hersbach H, Kobayashi S, Peubey C (2014) Estimating low-frequency variability and trends in atmospheric temperature using ERA-Interim. Q J R Meteorol Soc 140:329–353. https://doi.org/10.1002/qj.2317

Sinha SH, Narkhedkar SG, Mitra AK (2006) Barnes objective analysis scheme of daily rainfall over Maharashtra (India) on a mesoscale grid. Atmosfera 19:59–76

Thiel H (1950) A rank-invariant method of linear and polynomial analysis, part 3. Ned Akad Wet Proc 53:1397–1412

Tobin I, Berrisford P, Dunn RJH, Vautard R, McVicar TR (2014) [Global climate; atmospheric circulation; surface winds] land surface wind speed [in "State of the climate in 2013"]. Bull Am Meteorol Soc 95(7):S28–S29

Tuller SE (2004) Measured wind speed trends on the west coast of Canada. Int J Climatol 24:1359–1374. https://doi.org/10.1002/joc.1073

Vautard R, Cattiaux JL, Yiou P, Thepaut JN, Ciais P (2010) Northern Hemisphere atmospheric stilling partly attributed to an increase in surface roughness. Nat Geosci 3(11):756–761. https://doi.org/10.1038/NGEO979

Vautard R, McVicar TR, Thepaut JN, Roderic ML (2012) [Global climate; atmospheric circulation; surface winds] land surface winds and atmospheric evaporative demand [in "State of the climate in 2011"]. Bull Am Meteorol Soc 93(7):S6–S38

Wan H, Wang XL, Swail VR (2010) Homogenization and trend analysis of Canadian near-surface wind speeds. J Clim 23(5):1209–1225

Wu J, Zha JL, Zhao DM (2016) Estimating the impact of the changes in land use and cover on the surface wind speed over the East China Plain during the period 1980-2011. Clim Dyn 46:847–863. https://doi.org/10.1007/s00382-015-2616-z

Wu J, Zha JL, Zhao DM (2017a) Evaluating the effects of land use and cover change on the decrease of surface wind speed over China in recent 30 years using a statistical downscaling method. Clim Dyn 48(1):131–149. https://doi.org/10.1007/s00382-016-3065-z

Wu J, Zha JL, Zhao DM, Yang QD (2017b) Changes in terrestrial near-surface wind speed and their possible causes: an overview. Clim Dyn. https://doi.org/10.1007/s00382-017-3997-y

Wu J, Zha JL, Zhao DM, Yang QD (2017c) Effects of surface friction and turbulent mixing on long-term changes in the near-surface wind speed over the Eastern China Plain from 1981 to 2010. Clim Dyn. https://doi.org/10.1007/s00382-017-4012-3

Xu M, Chang CP, Fu CB, Qi Y, Robock A, Robinson D, Zhang HM (2006) Steady decline of East Asian monsoon winds, 1969-2000: evidence from direct ground measurements of wind speed. J Geophys Res-Atmos 111:D24111. https://doi.org/10.1029/2006JD007337

Yang XM, Li ZX, Feng Q, He YQ, An WL, Zhang W, Cao WH, Yu TF, Wang YM, Theakstone WH (2012) The decreasing wind speed in southwestern China during 1969-2009, and possible causes. Quat Int 263:71–84

You QL, Kang SC, Flugel WA, Pepin N, Yan YP, Huang J (2010) Decreasing wind speed and weakening latitudinal surface pressure gradients in the Tibetan Plateau. Clim Res 42:57–64. https://doi.org/10.3354/cr00864

Yue S, Wang CY (2002) Applicability of prewhitening to eliminate the influence of serial correlation on the Mann-Kendall test. Water Resour Res 38(6):1068–14-7. https://doi.org/10.1029/2001WR000861

Zha JL, Wu J, Zhao DM (2016) Changes of probabilities in different wind grades induced by land use and cover change in Eastern China Plain during 1980-2011. Atmos Sci Lett 17:264–269. https://doi.org/10.1002/asl.653

Zha JL, Wu J, Zhao DM (2017a) Effects of land use and cover change on the near-surface wind speed over China in the last 30 years. Prog Phys Geogr 41:46–67. https://doi.org/10.1177/0309133316663097

Zha JL, Wu J, Zhao DM, Yang QD (2017b) Changes of the probabilities in different ranges of near-surface wind speed in China during the period for 1970–2011. J Wind Eng Ind Aerodyn 169:156–167. https://doi.org/10.1016/j.jweia.2017.07.019

Zhu J, Liao H, Li J (2012) Increases in aerosol concentrations over eastern China due to the decadal-scale weakening of the East Asian summer monsoon. Geophys Res Lett 39(9):L09809. https://doi.org/10.1029/2012GL051428